

# Luminescence chronology and lithic technology of Tianhuadong Cave, an early Upper Pleistocene Paleolithic site in southwest China

Yue Hu<sup>a,b,†</sup>, Qijun Ruan<sup>c,†</sup>, Jianhui Liu<sup>c</sup>, Ben Marwick<sup>d</sup>, Bo Li<sup>b,e,\*</sup> 

<sup>a</sup>Department of Archaeology, Sichuan University, 29 Wangjiang Road, Chengdu 610064, China

<sup>b</sup>Centre for Archaeological Science, School of Earth and Environmental Sciences, University of Wollongong, Wollongong, New South Wales 2522, Australia

<sup>c</sup>Yunnan Institute of Cultural Relics and Archeology, Kunming, Yunnan 650118, China

<sup>d</sup>Department of Anthropology, University of Washington, Seattle, Washington 98105, USA

<sup>e</sup>ARC Centre of Excellence for Australian Biodiversity and Heritage, University of Wollongong, Wollongong, New South Wales 2522, Australia

\*Corresponding author at: Centre for Archaeological Science, School of Earth and Environmental Sciences, University of Wollongong, Wollongong, New South Wales 2522, Australia. E-mail address: bli@uow.edu.au (B. Li).

(RECEIVED April 16, 2019; ACCEPTED September 26, 2019)

## Abstract

Tianhuadong is a cave site located in the northwest of Yunnan Province, China. Since 2010, several surveys and one test excavation have yielded more than 1000 stone artifacts. The lithic assemblage shows some features of Levallois and Quina technologies, similar to those found in Middle Paleolithic sites in the Western Hemisphere. In this study, we summarize the lithic industry and propose a reliable chronology for the site using optically stimulated luminescence (OSL) dating of individual quartz grains extracted from sediments. We applied the standardized growth curve method to deal with the problem associated with the saturation in natural OSL signals in quartz. Our dating results yielded ages of 90–40 ka, suggesting that the associated lithic assemblage could be assigned to Marine Oxygen Isotope Stages 5 and 4 and could potentially represent Middle Paleolithic technologies. Because the number of Middle Paleolithic sites in southwest China is small, this site provides one of the few traces of human occupation in southwest China during the early upper Pleistocene. Thus, it is important for understanding hominin evolution and dispersal in this region.

**Keywords:** Southwest China; Middle Paleolithic; Luminescence dating; Single grain; Standardized growth curves

## INTRODUCTION

The timing and nature of the dispersal of archaic and modern humans out of Africa and into Asia, and their interactions with local hominin populations, are key questions in human evolution (Bae et al., 2017). The Eastern Hemisphere is especially important for answering these questions because of a long Pleistocene record of multiple hominin species, including *Homo erectus*, Denisovans, *Homo floresiensis*, and *Homo sapiens*, with *H. sapiens* potentially deriving from several dispersal events (Martínón-Torres et al., 2017). Previous work has claimed the primary event leading to the appearance of modern humans in Asia was a dispersal event out of Africa and into Eurasia around 50–60 ka (Marine Oxygen Isotope Stage [MIS] 3; Stringer and Andrews, 1988). Although a

dispersal event at this time was a substantial contributor to Pleistocene population structures in Asia (Prüfer et al., 2014), an accumulation of recent evidence from archaeology, hominin paleontology, geochronology, and genetics has complicated this account. Increasingly, evidence points to important dispersals out of Africa beginning during MIS 5 (130–71 ka), with archaeological evidence appearing in inland dispersal corridors (Petraglia et al., 2007, 2010; Liu et al., 2010; Demeter et al., 2012; Bae et al., 2014; Groucutt et al., 2015; Liu et al., 2015; Westaway et al., 2017).

For the major MIS 3 dispersal, two directional models are consistent with the evidence, broadly northerly and southerly paths (Kaifu et al., 2015). The paths taken by dispersals during MIS 4 and 5 are less clear, however. A southern coastal route has been suggested by genetic evidence (Macaulay et al. 2005), but most archaeological deposits from this period in India, China, Laos, Sumatra, and Philippines are located away from the coast. In addition, the technological behaviors that enabled the MIS 4 and 5 dispersals, especially into East Asia, remain unclear. Lithic assemblages in East Asia at this time are often described as showing little difference from

†These authors contributed equally to this study.

**Cite this article:** Hu, Y., Ruan, Q., Liu, J., Marwick, B., Li, B. 2019. Luminescence chronology and lithic technology of Tianhuadong Cave, an early Upper Pleistocene Paleolithic site in southwest China. *Quaternary Research* 1–16. <https://doi.org/10.1017/qua.2019.67>

Mode 1 technologies characterized by simple cores, flakes, and tools that lack standardization (Gao and Norton, 2002; Norton et al., 2009; Gao, 2013). These assemblages, by their absence of Mode 2 (characterized by bifacial retouched tools such as the hand axe) and Mode 3 (characterized by prepared core technologies such as Levallois concept) technologies, show little influence of dispersal events of hominins from Europe and western Asia. However, recent work on assemblages in southwest China is starting to indicate the presence of traces of technological innovation that might reflect population events such as dispersals or increases in the density and connectivity of MIS 4 and 5 groups in East Asia (Lycett and Norton, 2010).

Recent reassessment of the chronology and stone artifact technology at Guanyindong Cave in Guizhou Province, China, identified traces of the Levallois strategy dated to approximately 170–80 ka (Hu et al., 2019). Similarly, traces of Levallois have been described in the stone artifact assemblage from Lingjing (Henan Province, China), dated to 125–90 ka (Li et al., 2019). The Lingjing artifacts are associated with two archaic human crania demonstrating a mixture of traits from archaic East Asian humans, Neanderthals and early modern humans. Taken together, these two assemblages lend support to recognition of a Chinese Middle Paleolithic, as a regional variant of the Middle Pleistocene technological advances documented at Eurasian and African archaeological sites (Li et al., 2019). What makes the Chinese Middle Paleolithic distinct from the Middle Pleistocene assemblages in the Western Hemisphere is the low frequencies of prepared core technologies and pieces produced using a Levallois strategy. The rarity of Levallois in East Asia, relative to the Old World, may be because of small, low-density populations with weak and/or irregular patterns of social interconnectedness in this region during the Middle Pleistocene. Under these conditions, technological innovation or persistence would have been rarer, compared with the high-population and/or high-density conditions of Middle Pleistocene sub-Saharan Africa, where Levallois is more abundant (Lycett and Norton, 2010).

With only these two assemblages, the trajectory of technological evolution during MIS 5 and 4 in China is obscure because of the scarcity of Middle Pleistocene sites in this region and lack of reliable chronology. It is not until MIS 3 that another assemblage in China shows signs of Levallois and far to the north at Jinsitai Cave in Inner Mongolia. Levallois cores and points have been recovered from layers dated to ca. 47–42 ka (Li et al., 2018). This sparse archaeological record from MIS 5–4 in China makes it challenging to investigate models of hominin dispersals, contractions, extirpations, and extinctions during this important time. One reason for the sparseness of the record in China is that many sites with cultural materials in Pleistocene deposits have only been dated with radiocarbon methods; however, the ages of the dated materials are beyond the limit of radiocarbon dating (~50 ka).

In this article, we report on our dating of a recently discovered Paleolithic site from southwest China, Tianhuadong

(THD) Cave, using a newly developed optical dating technique. Optically stimulated luminescence (OSL) dating is suitable for establishing chronologies for sites older than 50 ka, because it can reach ages beyond the range of radiocarbon dating. First proposed in 1980s, optical dating provides an estimate of the time since mineral grains, such as quartz or feldspars, were last exposed to sunlight or heat (temperatures above 300°C) (Huntley et al., 1985; Aitken, 1998; Roberts et al., 2015). Over the last decade, it has been widely applied to determine the ages of Quaternary sediments all over the world (Preusser et al., 2008; Wintle, 2008; Rhodes, 2011; Roberts et al., 2015).

Our attempts to date the deposits at Tianhuadong using radiocarbon methods have not been successful because of the old age of the dated materials (>50 ka). Previously, research tentatively allocated the assemblage to MIS 5–4, because its lithic assemblage exhibits some characteristics that are comparable with Middle Paleolithic cultures from Europe and Africa (Ruan et al., 2017). We dated the artifact-bearing deposits using single-aliquot regenerative-dose (SAR) procedure for individual quartz grains extracted from the sediments. Our results confirm that the age of archaeological deposits at Tianhuadong falls into the MIS 5–4, providing new evidence of human activity during the Middle–Upper Pleistocene in this region.

## SITE AND STRATIGRAPHY

Tianhuadong (26°02.211'N, 100°27.648'E; 1805 m above sea level) is a cave site located on the east side of a limestone valley, Heqing County, Yunnan Province, southwest China (Fig. 1a). The cave, ~200 m long, has a 13-m-wide entrance. It covers an area of ~2400 m<sup>2</sup>. Sixteen kilometers to the north of the cave is the Jinsha River, and ~100 m to the west is a branch of the Caifeng River. This cave has been used as a temple for many years, so it is difficult to investigate and excavate inside the cave. For this reason, investigations were carried out in 2010, 2013, and 2016 on a gentle slope in front of the cave (Fig. 1b) by the Institute of Cultural Relics and Archaeology of Yunnan Province. A 1 × 2 m trench (T1), extending from west to east, was opened (Fig. 1c). The deposits excavated are mainly red silty clay with a stable and homogeneous sedimentary structure. The sedimentary profile of the trench was divided into five layers (Fig. 2), which are described as follows: (1) Layer 1 (0–25 cm thick) is a disturbed top soil layer. It consists of brown-yellow silty clay. A total of 81 stone artifacts and a small number of animal fossils were recovered from this layer. (2) Layer 2 was divided into two sublayers, layers 2a (15–40 cm thick) and 2b (35–70 cm thick). Layer 2a is a light-brown/red silty clay layer with dense structure and solid texture. Weak carbonate cementation is developed. A total of 100 stone artifacts were recovered from this layer. Layer 2b is a brown-red silty clay layer, with similar structure and texture as layer 2a. Only a few (n = 14) stone artifacts and animal fossil fragments were found from layer 2b. (3) Layer 3 (10–45 cm thick) consists of brown silty clay with carbonate

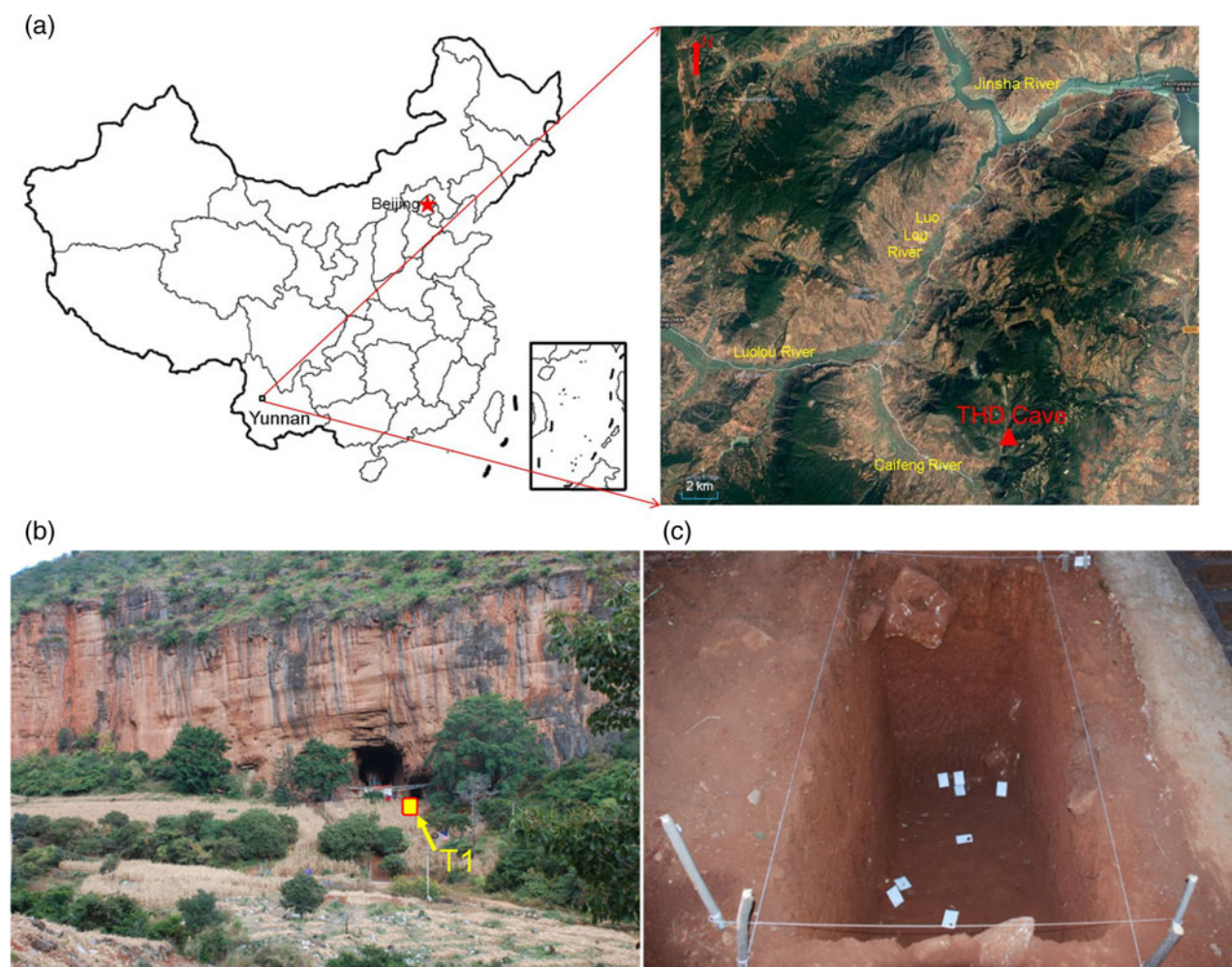


**Figure 1.** (color online) (a) Geographic locations of the Tianhuadong site. (b) Photo showing the cave entrance and the excavation area (T1) in front of the cave. (c) Photo showing the excavated trench.

cementation. It bears numerous ( $n = 56$ ) stone artifacts, animal fossil fragments, and some charcoal fragments. (4) Layer 4 (15–70 cm thick) is red-brown silty clay with carbonate cementation. Numerous animal fossil fragments and a small number ( $n = 32$ ) of stone artifacts were recovered. (5) Layer 5 (15–30 cm thick) is a brown-red silty clay layer with carbonate cementation. Only a small number of animal fossil fragments and charcoal fragments were recovered.

Apart from the top layers (1 and 2a), there is no obvious evidence of reworking induced by water flows. According to observations by local farmers, the deposits from the near surface ( $\sim 0.5$  m) were removed during previous engineering activities. Therefore, the stone artifacts collected from the surface are expected to originate from the overlying deposits that have been removed and the underlying deposits (mainly layer 1) that have been reworked during engineering activities. More than half of the stone artifacts and fossils recovered from both the surface and lower deposits show signs of weathering on their surface. This is probably because of the acid depositional environment associated with red clay, a typical depositional environment in south China. Most of the stone artifacts recovered from the deposits and collected

from the surface show little or no traces of abrasion on their edges, indicating that they were neither exposed for a long period nor transported for a long distance. This suggests that the artifacts were recovered in situ, although more detailed taphonomic work is needed to fully understand the site formation process.

## STONE ARTIFACTS

The detailed analysis of the stone artifacts from this site has been reported by Ruan et al. (2017), so here we only briefly summarize the key features of the assemblage to give context to the new OSL ages (see the next section). A total of 1121 stone artifacts including 289 from within the stratigraphic layers and 832 from the surface were studied. Table 1 summarizes the number of stone artifacts collected from individual cultural layers and surface. Most of the artifacts ( $n = 114$ ) came from layer 2, followed by layer 1 and then layer 3. The artifacts collected from the surface and individual layers show similar features in the extent of weathering, raw material, and typology. We could not identify any clear technological changes through different layers. This, however, does not rule

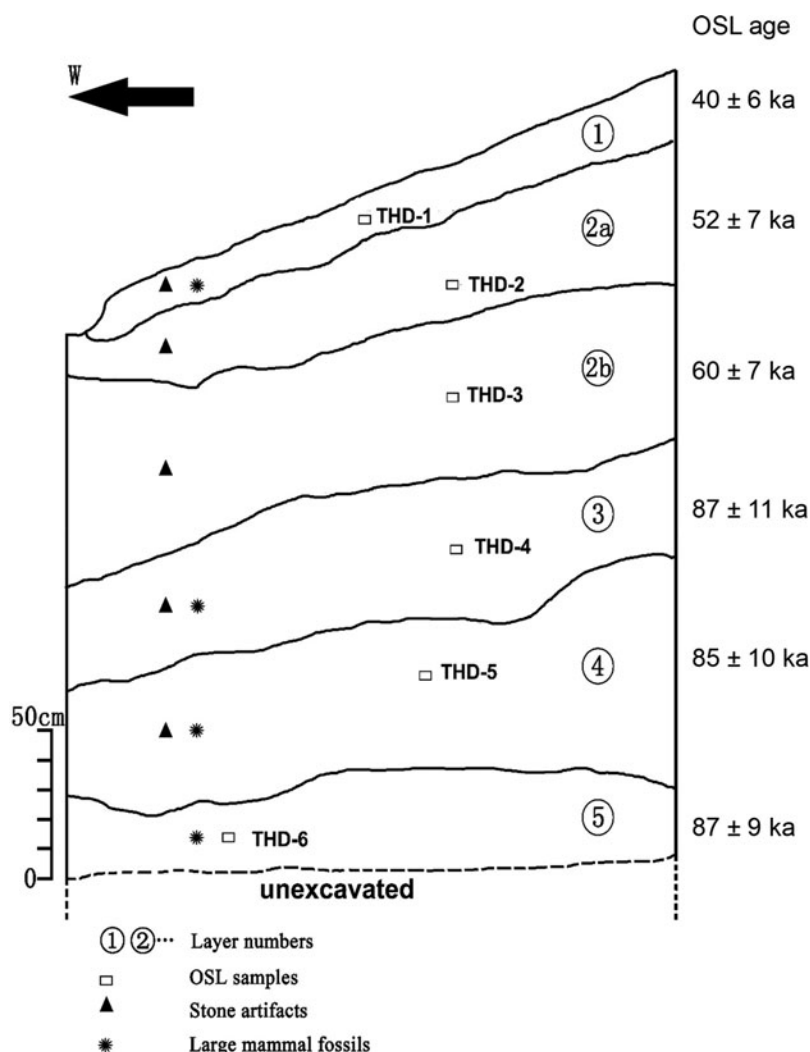


**Figure 2.** Schematic diagram of the stratigraphy, cultural relics and localities of optically stimulated luminescence (OSL) samples of the north wall of T1. Figure modified from Ruan et al. (2017).

out any systematic difference among different layers, because of the relative small number of artifacts excavated from individual layers. Further excavation may be able to provide more statistically significant information for studying the stratigraphic and chronological evolution in the stone technology. At this stage, we believe it is best to treat the stone artifacts from all layers

as a whole assemblage. The entire lithic assemblage consists of cores ( $n = 37$ ), flakes ( $n = 509$ ), tools ( $n = 113$ ), and chunks and debris ( $n = 462$ ). Hard hammer percussion is the dominant technique utilized. The raw materials are dominated by igneous rock (78%), and there appear to have been no major changes in preference in raw material selection over time.

**Table 1.** Statistics on the distribution of stone artifacts collected from cultural layers and surface in the Tianhuadong site.

Layer	Cores	Whole flakes	Flake fragments	Tools						Total	Proportion (%)
				Broken hammerstones	Scrapper	Quina-like scrapper	Denticulate	Notch	Debris		
Surface	33	317	70	2	33	35	27	4	311	832	74
1	2	43	5	0	0	2	0	1	28	81	7
2a	1	41	9	0	1	1	0	1	46	100	9
2b	0	7	0	0	1	0	1	0	5	14	1
3	1	8	3	0	3	1	0	0	40	56	5
4	0	4	2	0	0	0	0	0	32	38	3

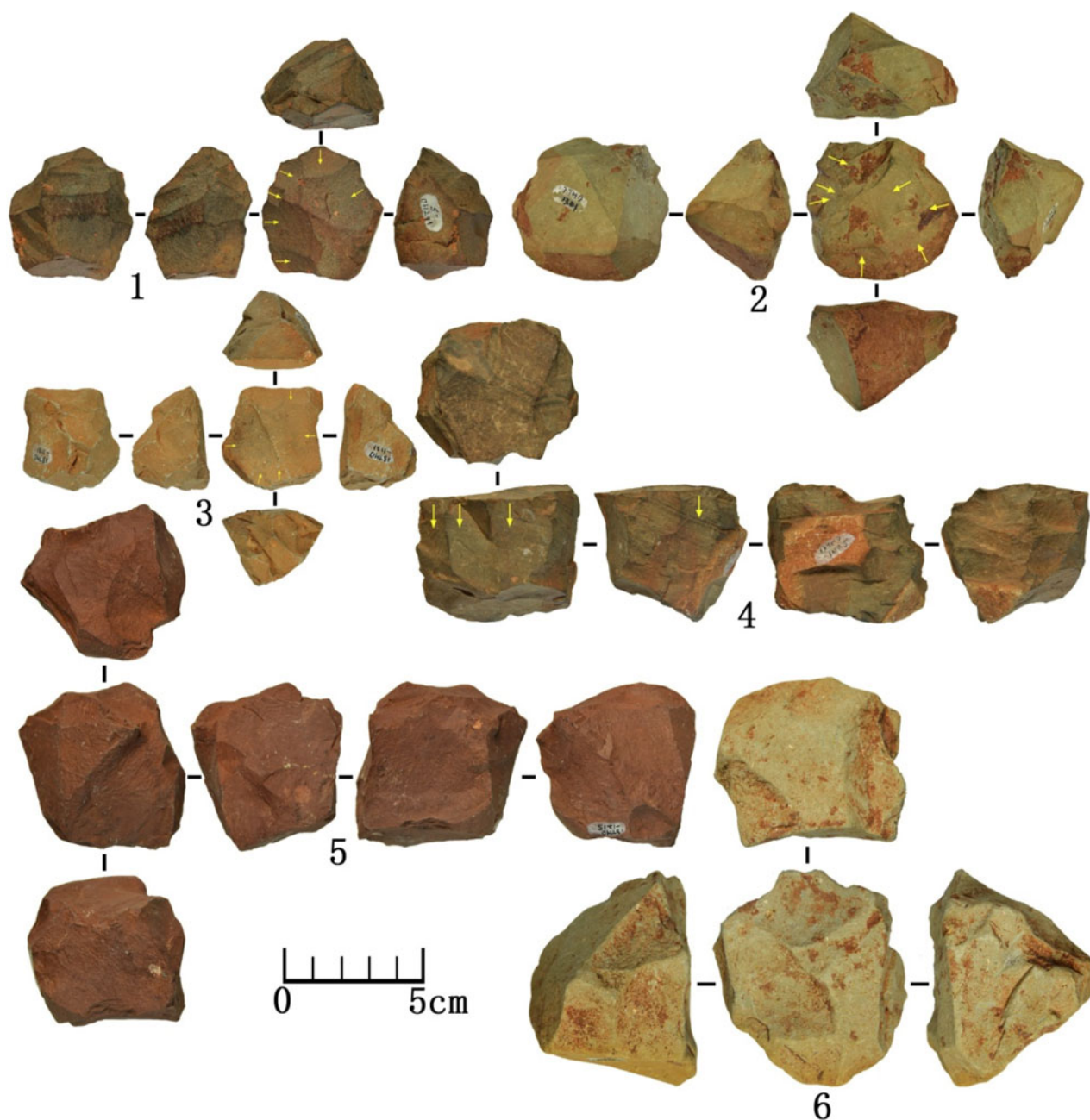


**Figure 3.** (color online) Photos showing selected cores from the THD site. 1, Discoidal core; 2–3, prepared cores; 4, multiplatform core with elongated flaking scars; 5–6, multiplatform cores. Photos from Ruan et al. (2017).

### Cores

Selected cores from the Tianhuadong site are shown in Figure 3. There are two types of core strategies, simple debitage and complex debitage. Cores that demonstrate no signs of preparation or predetermination were classified as the simple debitage (Fig. 3.1, 3.4–3.6). This type of core includes single platform, double platform, and multiplatform cores. Other cores show traces of preparation and predetermination or have a relatively stable morphology and reduction strategy representing complex debitage (Fig. 3.2–3.3). Most cores are knapped simply, yielding a constricted number of flakes with irregular morphologies. There are two cores that

resemble the Levallois reduction (Fig. 3.2–3.3) because of the recurrent centripetal scar pattern shown on the upper surface and other criteria such as hierarchical construction. However, a larger sample is needed to confirm the systematic, long-term use of Levallois strategies at this location. One core displays several parallel scars (Fig. 3.4).

### Flakes

Selected flakes are shown in Figure 4. There are 420 complete flakes, which comprise ordinary flakes, elongated flakes, crest flakes, discoidal flakes, Levallois-like flakes, and

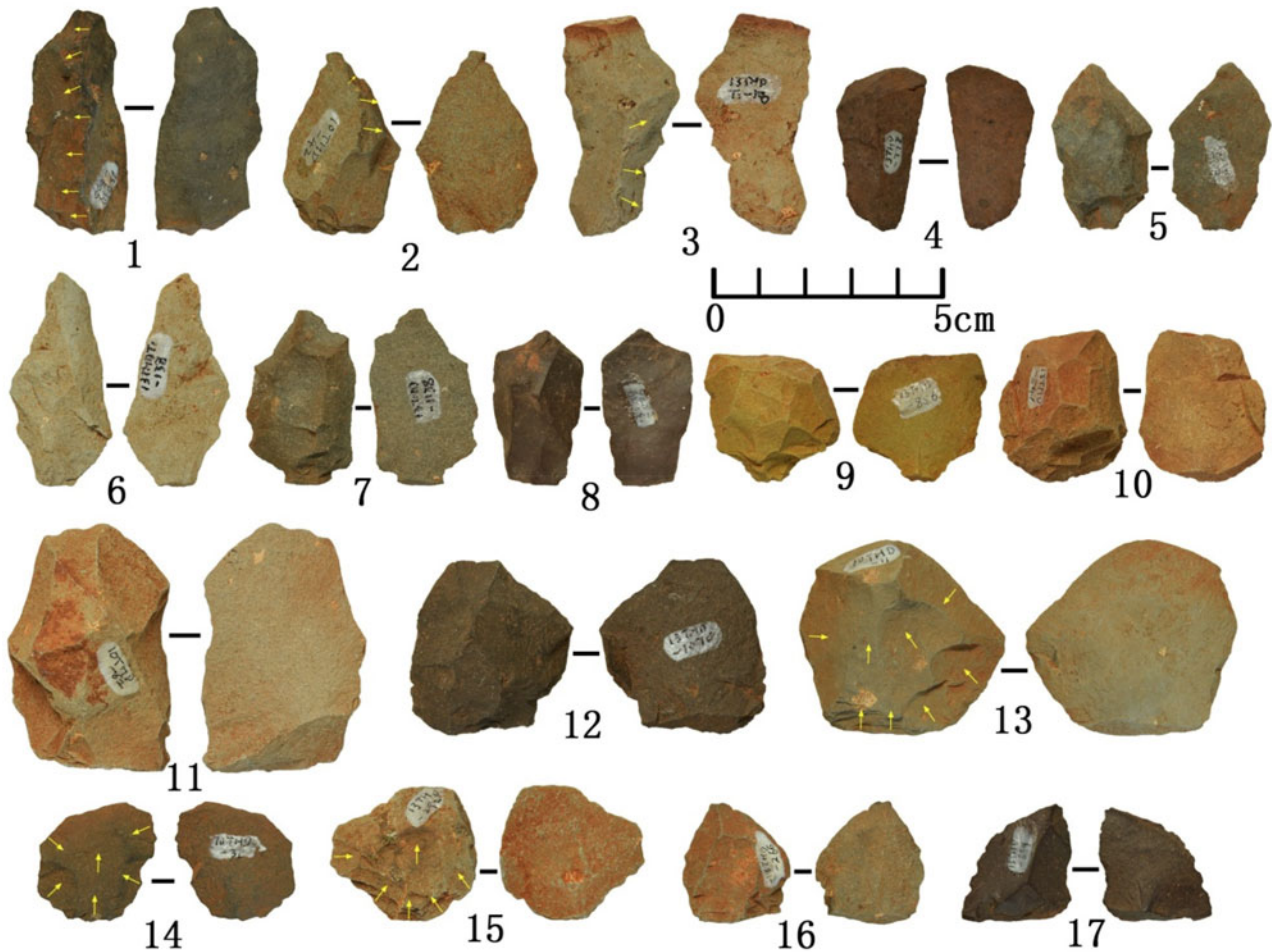


**Figure 4.** (color online) Selected flakes from the THD site. 1–3, Crested long flakes; 4–8, elongated flakes; 9–12, flakes produced from classic discoidal cores; 13–15, flakes with dorsal scar pattern resembling Levallois flakes; 16–17, triangular flakes. Photos from Ruan et al. (2017).

triangle flakes. There are 89 flake breaks including proximal, distal, and medial breaks, as well as left and right splits. Elongated flakes are defined as having a length dimension that is two times greater than the width dimension, with regular ridges on the dorsal side (Fig. 4.4–4.8). There are several flakes that have sharp edges and a thick center with centripetal ridges convergent in the middle (Fig. 4.9–4.12), which may have been produced from classic discoidal cores. There are a small number of flakes that demonstrate nearly elliptical shapes, centripetal dorsal scars, and other features that resemble the dorsal scar pattern of products obtained from Levallois reduction (Fig. 4.13–4.15).

## Tools

Tools make up 10% of the entire assemblage. They consist of hammers, sidescrapers, denticulates, and notches (see Fig. 5 for selected tools). The blanks of tools are mainly flakes or broken flakes. Most of them are small and with a low intensity of retouch, leading to irregular morphologies and edge shapes, as well as uneven retouching scars. There are only a few tools with extensive small retouching. Notably, there are 38 scrapers, which we term Quina-like scrapers

that exhibit similar features with Quina retouch scrapers found in Europe (Fig. 5). However, compared with Quina tools found in Europe, the scrapers are less standardized and show relatively little control over the shape of the cutting edge. Most are denticulate with irregular shapes. The retouch scars are relatively large, and lack a systematic pattern of repetition. Fine retouch is absent. These scrapers are larger than other types of tools and are retouched on thick blanks (most of them are flakes). The retouching scars are stepped and terminate in either step or hinge fractures. Compared with other tools, they have more intensive and invasive retouch and regular morphologies. The retouching scars are evenly distributed, ending up with more normative edge shapes.

## SAMPLES AND MEASUREMENT FACILITIES

### Sample description and preparation

A total of 6 sediment samples were collected for dating from each of the stratigraphic layers and sublayers from the north wall of the test trench (Fig. 2). The samples were collected by hammering opaque steel tubes, each about 5 cm in diameter and ~25 cm long, into the cleaned section face.



**Figure 5.** (color online) Selected Quina-like scrapers discovered in the THD site. 1–2, Discoidal retouched Quina-like scrapers; 3, multiedged Quina-like scraper; 4–7, semidiscoidal retouched Quina-like scrapers. Photos from Ruan et al. (2017).

The tubes were sealed in black plastic bags and transported to the University of Wollongong for analysis. The sample tubes were opened and prepared under dim red light in the OSL dating laboratory at the University of Wollongong. The materials at both ends of each tube were removed and used for

determining the environmental dose rate, because they might have been exposed to sunlight at the time of sample collection.

Quartz grains were extracted using standard preparation procedures (Aitken, 1985; Wintle, 1997). First, the samples

were dissolved in 10% hydrochloric acid to remove carbonate before they were subsequently treated with 30% hydrogen peroxide solution to remove organic matter. The remaining sample was dried and then sieved to isolate grains of 180–212  $\mu\text{m}$  in diameter. Quartz grains were separated from other minerals by density separation using sodium polytungstate solutions of 2.62 and 2.70 specific gravities, respectively. The separated quartz grains were etched with 48% hydrofluoric acid for  $\sim 40$  min to remove any feldspar contamination and to remove the outer layer of each quartz grain that was irradiated by alpha particles. The etched grains were then rinsed in hydrochloric acid to remove any precipitated fluorides, before being dried and sieved again to obtain grains of 180–212  $\mu\text{m}$  in diameter.

### Measurement facilities

All OSL measurements were made on an automated Risø TL-DA-20 luminescence reader equipped with a focused green laser (532 nm) (Bøtter-Jensen et al., 2003). Laboratory irradiations were carried out within the luminescence reader using a calibrated  $^{90}\text{Sr}/^{90}\text{Y}$  beta source. For OSL measurements, individual quartz grains were mounted onto standard Risø single grain discs (gold-plated aluminum discs drilled with 100 holes that are each 300  $\mu\text{m}$  in diameter and 300  $\mu\text{m}$  deep) (Bøtter-Jensen et al., 2000), where each grain hole contained 1 grain of 180–212  $\mu\text{m}$  in diameter. The spatial variation in the dose rate for individual grain positions was calibrated using gamma-irradiated calibration quartz standards. The ultraviolet OSL emissions were detected by an Electron Tubes Ltd. 9235QA photomultiplier tube fitted with a 7.5-mm Hoya U-340 filter.

### OSL DATING

OSL age is determined by dividing the equivalent dose ( $D_e$ , a measure of the radiation energy absorbed by grains during their period of burial) by the environmental dose rate (the rate of supply of ionizing radiation to the grains over the burial period). Analysis typically focusses on one of two minerals, quartz or K-feldspars. Quartz is commonly used

for dating when sediments are younger than  $\sim 200$  ka, whereas K-feldspar is used to date older samples because the infrared-stimulated luminescence signals from K-feldspar saturate at a much higher radiation dose than does the conventional OSL signal from quartz (Li et al., 2014). Our analysis found that K-feldspars are rare in the deposits at Tianhuadong, and the grains we sampled showed only a dim luminescence signal, which prevented us from applying K-feldspar for dating this site. As a result, we focused our analysis on the quartz minerals to determine the sedimentary ages of our sediment samples.

### Dosimetry

The environmental dose rate for etched quartz is attributable mainly to beta and gamma radiation, from the decay of  $^{238}\text{U}$ ,  $^{235}\text{U}$ , and  $^{232}\text{Th}$  (and their daughter products) and  $^{40}\text{K}$  in the deposits surrounding the dated grains, and cosmic rays. Beta dose rates were measured directly by low-level beta counting of dried, homogenized, and powdered sediment samples from the dosimetry bags, using a GM-25-5 multiscaler system (Bøtter-Jensen and Mejdahl, 1988). Gamma dose rates were measured based on the combination of thick source alpha counting and beta counting. The cosmic-ray dose rates were estimated following Prescott and Hutton (1994), based on the geomagnetic latitude and altitude of the site, as well as the thickness of sediment above each sample. Because our samples were collected immediately in front of a mountain (Fig. 1b), we also allowed for the overhead mountain shielding (i.e., the cosmic-ray dose rates are about 50% of those if there is no mountain shielding). We assigned a relative uncertainty of 10% to account for the systematic uncertainty in the primary cosmic-ray intensity.

The measured water contents of the six samples ranged from 10% to 16% (Table 2). Because these samples were stored for a few months after being taken, we expect that the measured present-day water contents were slightly underestimated. So, instead of using the in situ water content, we used a value of  $15 \pm 5\%$  as an estimate of the long-term water content for our OSL samples. The measured in situ water contents were within the 1-sigma range of the assumed

**Table 2.** Dose rate data, equivalent doses ( $D_e$ ) and optically stimulated luminescence (OSL) ages for sediment samples from the THD site.

Sample	Depth Layer (cm)	Grain size ( $\mu\text{m}$ )	Water content (%) <sup>a</sup>	Gamma dose rate (Gy/ka)	Beta dose rate (Gy/ka)	Cosmic ray (Gy/ka) <sup>b</sup>	Total dose rate (Gy/ka)	$D_e$ (Gy) <sup>c</sup>	Age (ka) <sup>c,d</sup>	
THD-OSL1	1	10	180–212	$15 \pm 5$ (12)	$1.84 \pm 0.42$	$1.93 \pm 0.11$	$0.150$	$3.92 \pm 0.43$	$158 \pm 17$	$40 \pm 6$
THD-OSL2	2a	30	180–212	$15 \pm 5$ (13)	$1.62 \pm 0.38$	$1.80 \pm 0.11$	$0.130$	$3.56 \pm 0.39$	$186 \pm 12$	$52 \pm 7$
THD-OSL3	2b	60	180–212	$15 \pm 5$ (12)	$1.52 \pm 0.32$	$1.72 \pm 0.11$	$0.115$	$3.36 \pm 0.34$	$202 \pm 9$	$60 \pm 7$
THD-OSL4	3	110	180–212	$15 \pm 5$ (10)	$1.48 \pm 0.31$	$1.60 \pm 0.09$	$0.110$	$3.18 \pm 0.33$	$277 \pm 17$	$87 \pm 11$
THD-OSL5	4	145	180–212	$15 \pm 5$ (15)	$1.57 \pm 0.28$	$1.88 \pm 0.12$	$0.105$	$3.55 \pm 0.30$	$300 \pm 22$	$85 \pm 10$
THD-OSL6	5	190	180–212	$15 \pm 5$ (16)	$1.62 \pm 0.32$	$1.92 \pm 0.11$	$0.100$	$3.64 \pm 0.34$	$317 \pm 15$	$87 \pm 9$

<sup>a</sup>Values used for dose rate and age calculations, with measured (field) water contents shown in parentheses.

<sup>b</sup>Values after correction for the zenith angular distribution of cosmic rays.

<sup>c</sup>The  $D_e$  and corresponding ages for THD-OSL1 and THD-OSL2 were based on maximum age model, but they should be considered as minimum ages.

<sup>d</sup>A systematic error of 2% was added (in quadrature) to the propagated random errors in the final ages to allow for any bias associated with calibration of the laboratory beta sources.

value. Each of the measured beta and gamma dose rates and the calculated cosmic-ray dose rate were corrected for attenuation by water using the assumed water content.

### Equivalent dose determination

The  $D_e$  values were determined using a SAR procedure (Supplementary Table 1) (Galbraith et al., 1999; Murray and Wintle, 2000). The SAR procedure involved measuring the OSL signals from the natural (burial) dose and from a series of regenerative doses, each of which was preheated at a given temperature (e.g., 240°C) for 10 s prior to optical stimulation by a green laser beam for 1 s at 125°C. A fixed test dose (~10 Gy) was given after each natural and regenerative dose, with the induced test dose OSL signals used to correct for any sensitivity changes during the SAR sequence. A cut-heat temperature (e.g., 180°C) lower than the preheat temperature was applied to the test dose. A duplicate regenerative dose was included in the procedure to check the validity of sensitivity correction, and a “zero dose” measurement was made to monitor the extent of any “recuperation” or “thermal transfer” induced by the preheat. We also applied the OSL infrared depletion-ratio test (Duller, 2003) at the end of the SAR sequence, using an infrared bleach of 100 s at 50°C, to check for feldspar contamination.

### SAR performance test

In order to find the most suitable experimental conditions (e.g., preheat and cut-heat temperatures), we conducted dose recovery tests using a range of preheat and cut-heat temperatures (280/180°C, 260/180°C, 240/180°C, 220/180°C, 200/160°C, and 180/160°C). Because our samples are dominated by bright grains (about half of the grains emit a detectable OSL signal; Supplementary Table 2), only one single-grain disc (100 grains) was measured for each preheat temperature. In this test, all the grains were bleached for ~30 min using a Dr Hönle solar simulator (model: UVA-CUBE 400). The bleached grains were then given a dose of ~100 Gy, before being measured using the SAR procedure with different preheat and cut-heat temperatures. To select reliable single-grain  $D_e$  results, we applied several rejection criteria similar to but slightly different from those proposed by Jacobs et al. (2006). Grains were rejected if they exhibited one or more of the following properties: (1) Test-dose signal ( $T_n$ ) was too weak (i.e., the initial intensity was below the instrument detection limit [ $3\sigma$  below the background intensity] and/or the relative standard error on the test dose net-signal was more than 20%). (2) There were high levels of recuperation (i.e., the ratio between the sensitivity-corrected OSL signals for the zero dose and the largest regenerative dose was less than 5% of the natural response). (3) There was a poor dose response curve (DRC) (i.e., the regenerative signals were too scattered to be well fitted with suitable functions). It should be noted that a bad recycling ratio or IR-OSL depletion ratio would also fall into this group, so we did not apply a separate rejection criterion on

recycling ratio. To assess the goodness-of-fit of the DRCs, we adopted the figure-of-merit (FOM) and reduced-chi-square (RCS) values (Peng et al., 2016; Peng and Li, 2017), which are defined as follows:

$$FOM(\%) = 100 \times \frac{\sum_{i=1}^n |y_i^o - y_i^f|}{\sum_{i=1}^n y_i^f} \quad (1)$$

and

$$RCS = \frac{1}{N - n} \times \sum_{i=1}^n \frac{(y_i^o - y_i^f)^2}{\sigma_i^2} \quad (2)$$

where  $y_i^o$  and  $y_i^f$  denote the  $i$ th observed and fitted values, respectively;  $N$  and  $n$  denote the number of observations and fitted model parameters, respectively; and  $\sigma_i$  is the standard error for the  $i$ th observation. We set upper limits of 10% for the FOM and 5 for the RCS criteria as recommended by Peng and Li (2017), which have been shown to be able to select grains with satisfactory DRCs. (4) The sensitivity-corrected natural OSL signal ( $L_n/T_n$ ) was statistically (at  $2\sigma$ ) equal to or greater than the saturation level of the corresponding DRC. The implementation of the rejection process was achieved using the built-in functions provided in the R package “numOSL” (Peng and Li, 2017).

Between 26 to 46 grains were accepted for each of the preheat temperatures after applying the rejection criteria. The measured to given dose ratios (or dose recovery ratios) were summarized as radial plots (Supplementary Figure 1a–f) for each of the preheat temperatures, respectively. We applied a central age model (CAM) (Galbraith et al., 1999) to calculate the weighted mean recovery ratios for each preheat temperature, and these were shown in each of the radial plots (Galbraith et al., 1999; Galbraith and Roberts, 2012). The distribution of the measured  $D_e$  values is tightly distributed around a central value, and overdispersion (OD) values are all statistically consistent with zero. The dose recovery results were plotted against the preheat temperature in Figure 6a. It shows a “plateau” region between 200°C and 260°C. The recovery ratios are statistically consistent with unity at  $1\sigma$  for the preheat temperatures at 220°C and 240°C, although the results from 200°C and 260°C are slightly lower than unity. There is significant overestimation and underestimation for the preheat temperatures of 180°C and 280°C, respectively.

### SAR $D_e$ determination

Based on the performance tests shown previously, we have chosen the preheat/cut-heat temperatures of 240°C/180°C for measuring  $D_e$  values for all of the samples. Figure 6b shows the natural OSL decay curves of 10 grains from THD-OSL6. The OSL intensity varies significantly from grain to grain (e.g., the net initial OSL intensity varies from a few tens of counts per 0.1 s to more than 10,000 counts per 0.1 s). Despite nearly half of the grains yielding a detectable OSL signal, about 20% of the grains contributed ~80%

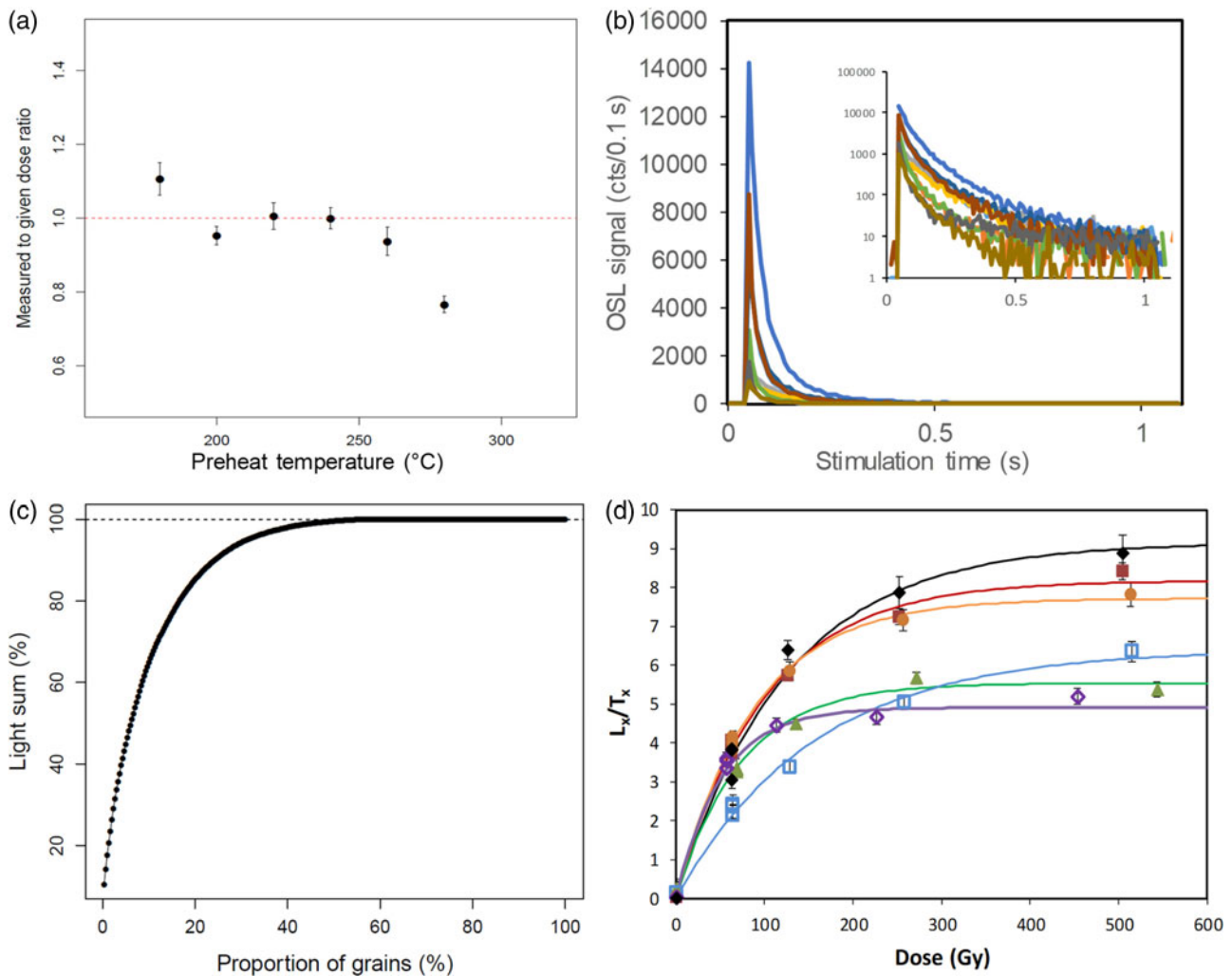


**Figure 6.** (color online) (a) The weighted mean dose recovery ratio plotted against preheat temperature. (b) Typical natural optically stimulated luminescence (OSL) decay curves of 10 grains of sample THD-OSL6. (c) Distribution of OSL signal intensities from 200 grains of quartz from sample THD-OSL6. Data are plotted as the proportion of the total light sum that originates from the specified percentage of grains. (d) Typical dose response curves from 6 grains of sample THD-6. The sensitivity-corrected ( $L_x/T_x$ ) dose response curves were well fitted using a single saturating exponential function of the form  $I = I_0(1 - \exp^{-D/D_0})$ , where  $I$  is the  $L_x/T_x$  value at regenerative dose  $D$ ,  $I_0$  is the saturation value of the exponential curve, and  $D_0$  is the characteristic saturation dose.

of the total OSL signal (Fig. 6c). Apart from the variation in OSL intensity, the DRCs from different grains also display a wide range of shapes associated with different saturation doses (Fig. 6d).

Between 500 and 800 grains were measured to determine  $D_e$  values for each of the samples, respectively. The same rejection criteria described previously were applied to select reliable results. The rejected grains number of each criterion is summarized in Supplementary Table 2. About 60% of the grains were rejected because of weak signals (i.e., the initial intensity of  $T_n$  was less than  $3\sigma$  above the background intensity and/or its relative standard error was more than 20%). Only a few grains of each sample were rejected because of recuperation larger than 5%. Among the grains with detectable OSL signals, from 23% to 49% of them were rejected because their DRC data were too scattered to be fitted reliably. We found that there was no discernable difference in the

brightness ( $T_n$ ) between the grains with satisfactory DRCs and those with poor DRCs. For those grains with satisfactory DRCs, however, there were significant proportions of grains (from 15% up to 57%) that had natural signals saturated. In other words, their  $L_n/T_n$  values were consistent or above the saturation levels of the corresponding DRCs, so that they yielded infinite  $D_e$  estimates or  $D_e$  error. After rejection of these grains, from 10% to 36% of the measured grains yielded reliable and finite  $D_e$  estimates.

The distributions of individual  $D_e$  values passed through the rejection criteria are shown in radial plots in Figure 7 for all of the samples. It can be seen that all of the samples have a broad range of  $D_e$  values, including many values close to zero, indicating that all the samples were affected by postdepositional mixture or intrusion of “younger” grains. This is especially apparent in the two uppermost samples (THD-OSL1 and THD-OSL2), which is not surprising

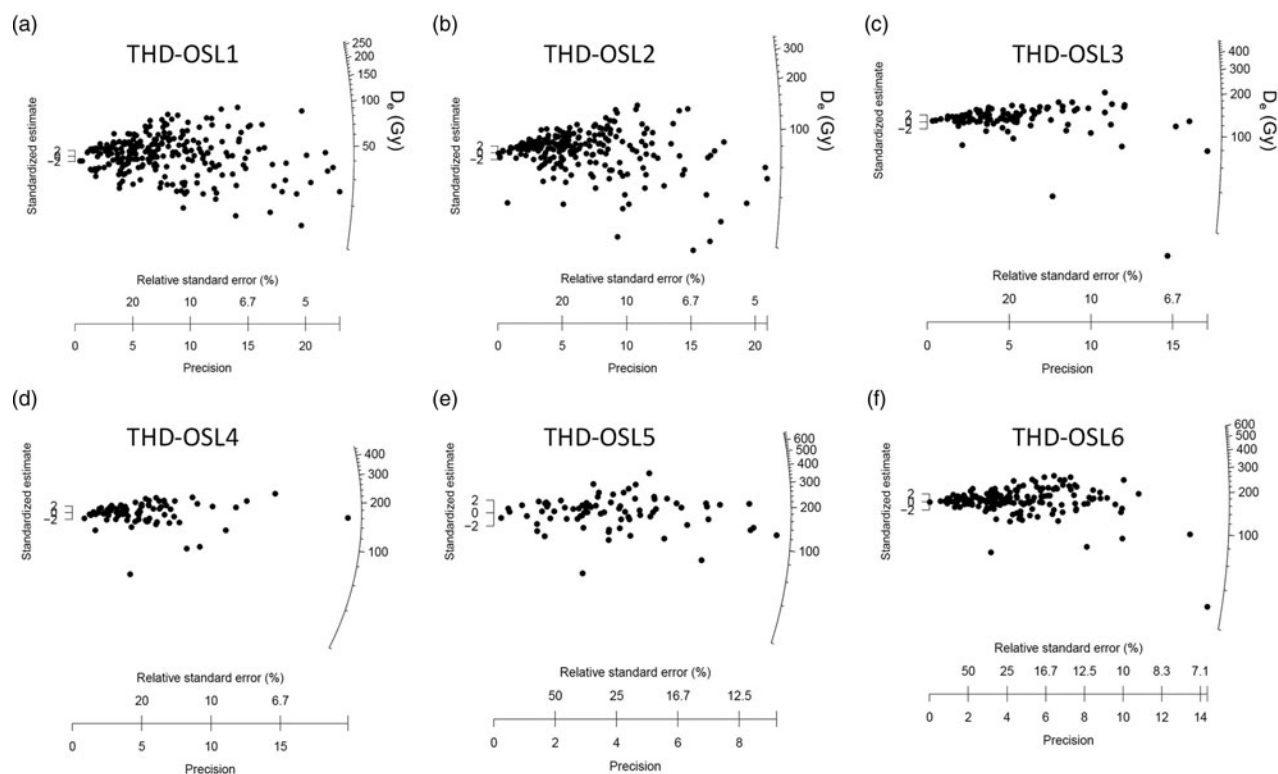


**Figure 7.** SAR  $D_e$  distribution of samples (a–f).  $D_e$  distribution for the accepted grains of samples THD-OSL1 to THD-OSL6, respectively. OS�, optically stimulated luminescence; SAR, single-aliquot regenerative-dose.

because the top layers have been disturbed by recent agricultural and engineering activities that might inevitably result in the mixture of younger and old grains in the upper layers and the intrusion of some young grains into the deeper layers. Fortunately, the intensity of mixing decreases significantly in the lower layers, which is demonstrated by the significant reduction in the number of younger grains in the four lower samples (THD-OSL3, THD-OSL4, THD-OSL5, and THD-OSL6).

### Standardized growth curve analysis

As shown in Supplementary Table 2, there are considerable proportions of grains (up to ~57%) that have natural signals being saturated, especially for the lower samples. It has been suggested by recent studies that the rejection of a large number of “saturated” grains may cause final  $D_e$  values to be considerably underestimated because of the truncation of the full  $D_e$  distribution (Duller, 2012; Thomsen et al., 2016; Guo et al., 2017; Li et al., 2017). To deal with this problem, a new method of analyzing the  $L_n/T_n$  distribution and establishing standardized growth curves (SGCs) (Roberts and Duller, 2004; Li et al., 2015) for different grains or aliquots has been proposed by Li et al. (2017). When using this method, because grains that are saturated are also accepted, it can obtain a full and untruncated distribution of the  $L_n/T_n$  ratios with a reliable  $D_e$  estimation beyond the conventional limit of  $\sim 2D_0$  using the standard SAR procedure. This method has been successfully applied to date the

Guanyindong Cave site from southwest China (Hu et al., 2019). Given the large number of “saturated” grains in our samples, the same method was applied to estimate  $D_e$  values of our samples.

First of all, the variability of the DRCs of our samples was investigated. We first identified and rejected poorly behaved grains, so that only well-behaved grains with reliable growth curves were analyzed. This was achieved based on the same rejection criteria mentioned previously, but the DRCs from “saturated” grains were accepted. In Supplementary Figure 2a, we have summarized the DRCs ( $n = 1464$ ) that passed the rejection criteria for all of the samples. From the figure, we can see that it is impossible to establish a common DRC for all of the grains because these DRCs are greatly variable among different grains, indicating that there are multiple groups of grains with different shapes of DRCs. Li et al. (2016) found that, according to different saturated dose levels, the single-grain DRCs for their quartz samples could be divided into three groups—namely, “early”, “medium,” and “later”—by analyzing the  $L_x/T_x$  ratios between two regenerative doses. In addition, the grains from the same group are characterized by a similar shape of DRC, so a single SGC can be established for each group. Following their method, we calculated the ratios between the  $L_x/T_x$  values from a large regenerative dose (400 Gy) and a smaller regenerative dose (100 Gy), which can reflect the saturation dose level of the corresponding DRC (e.g., higher ratios means later saturation, and smaller ratios mean early saturation). The ratios for individual grains from all of

the samples are shown in Supplementary Figure 2b. A large range of ratios from  $\sim 1$  to  $\sim 2.5$  is observed, indicating that the grains have a wide range of saturation doses. For example, the grains with  $L_x/T_x$  ratios close to 1 correspond to early saturated grains (i.e., there was a negligible increase in OSL signal beyond 100 Gy). In contrast, grains with higher  $L_x/T_x$  ratios have a larger saturation dose level.

In order to statistically identify the number of groups of grains that share similar DRC shapes (or  $L_x/T_x$  ratios), as well as estimate the weighted mean ratios for each group, we applied the finite mixture model (Galbraith and Green, 1990; Roberts et al., 2000; Galbraith and Roberts, 2012) to the  $L_x/T_x$  ratios. We found that, unlike what was observed by Li et al. (2016), at least seven groups were needed to fully take into account the observed spread in the ratios for our samples (Supplementary Fig. 2b). In order to establish corresponding SGCs for each of the groups (Supplementary Fig. 2c), a least-square normalization (LS-normalization) procedure (Li et al., 2016) was used to analyze the DRCs from each group, which involved the following steps: (1) fitting the  $L_x/T_x$  data from all grains from the same group using a best-fit model (e.g., single saturating exponential function); (2) rescaling the  $L_x/T_x$  data from each grain by multiplying a scaling factor so that the difference between rescaled  $L_x/T_x$  values from that grain and the fitted common growth curve was minimized through an optimization procedure (each grain was treated individually so different scaling factors were determined for different grains); (3) repeating steps 1 and 2 iteratively until there was negligible change in the rescaled regenerative-dose signals and best-fit function. The scaling factors obtained for individual grains were then used to normalize their corresponding natural signals ( $L_n/T_n$ ). The general order kinetic function (Guralnik et al., 2015) was used to fit the dose-response data from the same groups. The grouping of grains and establishment of SGC for each group were achieved using the combination of the two packages “numOSL” (Peng et al., 2013; Peng and Li, 2017) and “Luminescence” (Kreutzer et al., 2012) in R (R Core Team, 2016).

The SGCs for all of the groups are shown in Supplementary Figure 2c. It can be seen that different groups have considerably different saturation dose levels (i.e., group 1 saturated at  $\sim 100$  Gy, but group 7 showed no sign of saturation up to 600 Gy). To test the validity of grouping and SGC establishment, the ratios between the measured  $L_x/T_x$  and the expected values based on the SGC were calculated. The data show that they are statistically consistent with unity for all of the groups; most of these ratios ( $\sim 90\%$  or more) are consistent with unity at  $2\sigma$  (Supplementary Fig. 2d–j), supporting that the SGCs obtained are reliable. The proportions of grains in each DRC group are shown in Supplementary Figure 2k for each sample. It is shown that groups 2, 3, 4, and 5 are dominant in our samples, followed by group 1 and then group 6. Only a small proportion (less than 3%) of grains falls into group 7 for THD-OSL1, THD-OSL2, THD-OSL3, and THD-OSL4, but they are absent in THD-OSL5 and THD-OSL6.

## **$D_e$ determination based on SGCs**

In order to estimate  $D_e$  values for individual groups, we followed the method of Li et al. (2016) by analyzing the  $L_n/T_n$  values for each group. To allow direct comparison of natural signals among grains from the same group, the  $L_n/T_n$  values of each group were renormalized using the same scaling factors obtained during the LS-normalization procedure when the SGCs were established for individual groups. Statistical analysis was then conducted to the LS-normalized  $L_n/T_n$  values for each group to estimate their “weighted mean” value. Such value was then projected onto the corresponding SGC to estimate the final  $D_e$  for that group. The distribution of LS-normalized  $L_n/T_n$  values for individual groups of our samples is shown in Supplementary Figures 3–8, respectively.

Similar to the SAR  $D_e$  distribution shown in Figure 7a and b, the  $L_n/T_n$  distributions for the topmost samples THD-OSL1 and THD-OSL2 show a wide range of values, although a large proportion of the data points are clustered in the upper range, indicating that these samples were affected by intrusion of younger grains. So we applied the maximum age model (Olley et al., 2006), adapted from the minimum age model of Galbraith et al. (1999), to estimate the maximum component in the distribution. In this model, we used a value of 0.15 for  $\sigma_b$ , a parameter representing the expected overdispersion for a well-bleached and nondisturbed sample. This value is based on the OD values of the  $L_n/T_n$  distribution for the lower samples, in which no evidence of postdepositional mixture was observed (e.g., group 5 of THD-OSL5 shown in Supplementary Fig. 7e). For the 4 lower samples, all of the groups appear to have  $L_n/T_n$  values concentrated in a single population, although most of them contain a few grains that have considerably smaller  $L_n/T_n$  values. For this reason, we applied the normalized median absolute deviation (nMAD) method to reject outliers. We used 1.4826 as the appropriate correction factor for a normal distribution and rejected  $\log L_n/T_n$  values with nMADs greater than 1.5. This method is effective to reject outliers from the distribution (Supplementary Fig. 5–8). After rejecting the outliers using the nMAD method, we calculated the weighted mean values of the accepted data points based on the CAM.

The best estimates of  $L_n/T_n$  values based on our statistical analysis mentioned previously were then projected onto the corresponding SGCs to calculate  $D_e$  values for individual groups, which are summarized in Supplementary Table 3. For some groups (e.g., groups 6 and 7), insufficient numbers of grains were accepted, so reliable results could not be obtained. Group 1 (i.e., the early saturated group) of most samples and groups 2 and 3 from some samples yielded infinite  $D_e$  values because their  $L_n/T_n$  values are statistically consistent with the saturation levels of the corresponding SGCs. For the other groups that had higher saturation doses, finite results were obtained, and their  $D_e$  values were statistically indistinguishable from each other for the same sample. This further confirmed that the grouping, SGC establishment, and  $D_e$  estimates based on  $L_n/T_n$  and SGC were reliable. We, therefore, estimated the final  $D_e$  values

for each sample based on the weighted mean of the results of the DRC groups that produced finite  $D_e$  values (Table 2 and Supplementary Table 3). The dose rates, final  $D_e$  estimates, and ages for all of the OSL samples are summarized in Table 2.

## RESULTS

Based on the single grain analysis of samples from Tianhuadong, the two samples (THD-OSL1 and THD-OSL2) taken from the top layers contain a large number of younger grains, but the number of younger grains decreased progressively with the depth. This result is consistent with the fact that the top of the trench was used as agricultural land and reworked by engineering activities, resulting in numerous younger grains having intruded into the top layers. This suggests that single-grain measurements were able to effectively identify mixture in the deposits for the THD site. Furthermore, it is shown that the postdepositional mixture, as a result of agricultural and engineering activities, mostly affected the two uppermost samples and was insignificant for the lower samples (Supplementary Figs. 5–8).

The ages for our samples from Tianhuadong follow stratigraphic order, indicating good stratigraphic integrity of the deposit and the reliability of the age measurements. There is no obvious evidence of significant sedimentary hiatus, as indicated from stratigraphy and OSL ages. Sample THD-OSL6 from layer 5, which is archaeologically sterile, was dated to  $87 \pm 9$  ka. Sample THD-OSL5 from layer 4, associated with both artifacts and fossils, reveals the earliest human occupation at the THD site at  $85 \pm 10$  ka. The two samples (THD-OSL1 and THD-OSL2) taken from the top-most layers yielded ages of  $\sim 40$ – $50$  ka, suggesting that that human occupation of the site spans about 40–90 ka, corresponding to MIS 3–5c. Previous studies have suggested that southwest China had experienced cycles of glacial and interglacial periods during late Middle Pleistocene, broadly consistent with MIS stages (Hodell et al., 1999; Wang et al., 2004; Karkanas et al., 2008). During this period, global climate records indicate several glacial and interglacial cycles leading to temperature and environmental fluctuations (Lisiecki and Raymo, 2005). Nonetheless, according to the analysis of stone artifacts from Tianhuadong (Ruan et al., 2017), there were no major changes in the lithic technology and raw materials during this time span, indicating that the relationship between environmental changes and stone artifact technologies was weak during this time. We suggest that the technological strategies used at Tianhuadong were sufficient to be equally effective under a wide range of environmental conditions.

## DISCUSSION

According to our previous study (Ruan et al., 2017), the technologies of the Tianhuadong assemblage indicate a mix of simple and complex reduction. Generally, the lithic assemblage is similar to other MIS 4 and 5 sites found in

southwest China, with simple knapped cores and flake tools, such as Bianbiandong (upper Pleistocene; Cai et al., 1991), Yanhuadong (113–181 ka; Wu et al., 1975), and Xiaohuidong (49–55 ka; Cao, 1978). Core reduction is generally simple and without preparation in these assemblages. Retouch techniques at Tianhuadong are mainly simple knapping along the edge of flakes, consistent with other sites from the same region, such as Xiangbidong ( $\sim 50$  ka; Dali Bai Autonomous Prefecture Cultural Relics Management Institute, Yunnan Institute of Cultural Relics and Archeology, Jianchuan Institute of Cultural Relics, 2015), Yushuiping (40–20 ka; Gao et al., 2012), Laohudong (30–18 ka; Zhu and Ji, 2010), and Longtanshang locality 2 ( $\sim 30$  ka; Qiu and Zhang, 1985).

The Tianhuadong assemblage also exhibits characters that are similar to Middle Paleolithic cultures from Europe, Africa, and west Asia. The discovery of elongated flakes, crested flakes, and core with parallel scars indicates the development of blade technology in this region. The appearance of Levallois-like products at Tianhuadong is consistent with other nearby sites (e.g., Guanyindong and Panxiandadong) in southwest China that contain Levallois elements (Huang et al., 1997; Otte et al., 2017; Hu et al., 2019). Additionally, the Quina-like scrapers, representing a relatively complex retouching technique, are also similar to those from the Middle Paleolithic sites from Europe and Africa. Compared with late Middle Pleistocene sites, Panxiandadong ( $\sim 300$  to 130 ka; Huang et al., 1997; Miller-Antonio et al., 2004; Otte et al., 2017) and Guanyindong ( $\sim 170$  to 80 ka; Li and Wen, 1986; Leng, 2001; Li et al., 2009; Hu et al., 2019), Tianhuadong shares many similarities in tool making, such as core-flake tools and hard hammer percussion. However, neither raw material procurement nor exploitation, core preparation, invasion, and regularity of retouch at Tianhuadong are as complex and systematically present throughout the assemblage as found at Panxiandadong and Guanyindong.

In addition to the Levallois-like core and Quina-like retouched tools, the majority of the stone artifacts from Tianhuadong also exhibit various type of scrapers, denticulates, and notches resulting from invasive retouch on some of the tools. However, the small number of stone artifacts recovered from Tianhuadong prevents a comprehensive comparison with other assemblages. Levallois elements have also been reported from a younger site Dahe (44–35 ka; Ji, 2008) in the same region, indicating there might be a long-term technological transmission or population interaction in southwest Asia during the late Middle Pleistocene. Based on available information, we could draw a preliminary sketch for the late Pleistocene of semi-isolated human groups learning some technologies from their forebears or neighbors, with small numbers of these Levallois elements persisting through time. One reason why these technologies did not become more dominant in archaeological assemblages may be because of the low availability of raw materials with predictable flaking qualities (e.g., chert is rarely available in this region). Another contributing factor may be the constraints of relatively smaller effective population sizes that

limit the propagation and long-term persistence of new technologies (Lycett and Norton, 2010).

Although the record remains sparse, the results from Tianhuadong highlight the importance of the MIS 5 dispersal out of Africa. One possible implication of the finds at Tianhuadong is that the MIS 5 dispersal potentially resulted in the appearance of Levallois in East Asia. A second implication is that a southern, or lower-latitude, MIS 5 dispersal route may now be more plausible. However, Levallois itself is not sufficient evidence of this dispersal because it can be linked to both archaic and modern humans. Furthermore, Levallois strategies could result from convergent evolution, unrelated to dispersal events. Also, we currently lack fossil evidence to robustly link the appearance of Levallois in southwest China to a dispersal event. Hopefully, future work will lead to skeletal or ancient DNA evidence that can indicate how isolated or connected the human populations were in southwest China.

## CONCLUSION

Tianhuadong is important because it provides securely dated new evidence of human activity in southwest China during MIS 4 and 5. There are few Paleolithic sites in southwest China dating back to this period, compared with north China where there are more sites and where many have been intensively studied. Many of the sites in southwest China were dated in the last century, and the quality of dating results is difficult to assess because of the limited information provided in those publications. Ages at many of the sites were based only on stratigraphic correlation, without confirmation from absolute dating methods. This makes it challenging to understand human behavior and technological change during the Middle and Upper Pleistocene in this region.

Our OSL dating on individual quartz grains from sediments suggests that the age of archaeological deposits at Tianhuadong is approximately 40–90 ka. The lithic industry shows a diversity of lithic technologies and knapping strategies that are similar to those found from nearby Paleolithic sites in southwest China. The presence of features similar to Levallois and Quina technologies at Tianhuadong hints at population interactions among modern human groups following their initial appearance in East Asia during this period. Further archaeological and chronological studies in this region are, however, needed to better understand the trajectory of human behavior, evolution, and technology development during MIS 4 and 5 in this region.

## ACKNOWLEDGMENTS

This work was supported by the Australian Research Council through Future Fellowships to BL (FT140100384) and postgraduate scholarships from the University of Wollongong to YH. We thank Sam Lin for his constructive advice; Zenobia Jacobs, Yasaman Jafari, and Terry Lachlan for help in the laboratory; and Ashok Singhvi and an anonymous reviewer for their helpful comments.

## SUPPLEMENTARY MATERIAL

The supplementary material for this article can be found at <https://doi.org/10.1017/qua.2019.67>.

## REFERENCES

- Aitken, M.J., 1985. *Thermoluminescence Dating*. Academic Press, London.
- Aitken, M.J., 1998. *An Introduction to Optical Dating*. Oxford University Press, Oxford.
- Bae, C.J., Douka, K., Petraglia, M.D., 2017. On the origin of modern humans: Asian perspectives. *Science* 358, eaai9067.
- Bae, C.J., Wang, W., Zhao, J., Huang, S., Tian, F., Shen, G., 2014. Modern human teeth from Late Pleistocene Luna Cave (Guangxi, China). *Quaternary International* 354, 169–183.
- Bøtter-Jensen, L., Andersen, C.E., Duller, G.A.T., Murray, A.S., 2003. Developments in radiation, stimulation and observation facilities in luminescence measurements. *Radiation Measurements* 37, 535–541.
- Bøtter-Jensen, L., Bulur, E., Duller, G.A.T., Murray, A.S., 2000. Advances in luminescence instrument systems. *Radiation Measurements* 32, 523–528.
- Bøtter-Jensen, L., Mejdahl, V., 1988. Assessment of beta-dose-rate using a GM multiscaler system. *Nuclear Tracks and Radiation Measurements* 14, 187–191.
- Cai, H., Wang, X., Xu, C., 1991. Paleolith of Bianbian cave at Bijie County, Guizhou Province. *Acta Anthropologica Sinica* 10, 50–57.
- Cao, Z., 1978. Palaeolithic site found in Xiaohuidong cave at Shui-cheng, Guizhou Province. *Vertebrata Palasiatica* 16, 67–72.
- Dali Bai Autonomous Prefecture Cultural Relics Management Institute, Yunnan Institute of Cultural Relics and Archeology, Jianchuan Institute of Cultural Relics, 2015. *Study of the Jianchuan Xiangbidong Paleolithic Site*. Cultural Relics Publishing House, Beijing.
- Demeter, F., Shackelford, L.L., Bacon, A.M., Durringer, P., Westaway, K., Sayavongkhamdy, T., Braga, J., et al., 2012. Anatomically modern human in Southeast Asia (Laos) by 46 ka. *Proceedings of the National Academy of Sciences of the United States of America* 109, 14375–14380.
- Duller, G.A.T., 2003. Distinguishing quartz and feldspar in single grain luminescence measurements. *Radiation Measurements* 37, 161–165.
- Duller, G.A.T., 2012. Improving the accuracy and precision of equivalent doses determined using the optically stimulated luminescence signal from single grains of quartz. *Radiation Measurements* 47, 770–777.
- Galbraith, R.F., Green, P.F., 1990. Estimating the component ages in a finite mixture. *Nuclear Tracks and Radiation Measurements* 17, 197–206.
- Galbraith, R.F., Roberts, R.G., 2012. Statistical aspects of equivalent dose and error calculation and display in OSL dating: an overview and some recommendations. *Quaternary Geochronology* 11, 1–27.
- Galbraith, R.F., Roberts, R.G., Laslett, G.M., Yoshida, H., Olley, J.M., 1999. Optical dating of single and multiple grains of quartz from jinnium rock shelter, northern Australia: part 1, experimental design and statistical models. *Archaeometry* 41, 339–364.
- Gao, F., Min, R., Li, B., Duan, C., 2012. The significance of the first archaeological excavation of Yushuiping sites in Nujiang. In:

- Zhang, Y., Li, S. (Ed.), *The Nu Nationality in the Canyon*. Yunnan University Press, Kunming, Yunnan Province, China.
- Gao, X., 2013. Paleolithic cultures in China: uniqueness and divergence. *Current Anthropology* 54, S358–S370.
- Gao, X., Norton, C.J., 2002. A critique of the Chinese 'Middle Palaeolithic'. *Antiquity* 76, 397–412.
- Groucutt, H.S., Petraglia, M.D., Bailey, G., Scerri, E.M.L., Parton, A., Clark-Balzan, L., Jennings, R.P., et al., 2015. Rethinking the dispersal of *Homo sapiens* out of Africa. *Evolutionary Anthropology* 24, 149–164.
- Guo, Y.J., Li, B., Zhang, J.F., Yuan, B.Y., Xie, F., Roberts, R.G., 2017. New ages for the Upper Palaeolithic site of Xibaimaying in the Nihewan Basin, northern China: implications for small-tool and microblade industries in north-east Asia during Marine Isotope Stages 2 and 3. *Journal of Quaternary Science* 32, 540–552.
- Guralnik, B., Li, B., Jain, M., Chen, R., Paris, R.B., Murray, A.S., Li, S.H., Pagonis, V., Valla, P.G., Herman, F., 2015. Radiation-induced growth and isothermal decay of infrared-stimulated luminescence from feldspar. *Radiation Measurements* 81, 224–231.
- Hodell, D.A., Brenner, M., Kanfoush, S.L., Curtis, J.H., Stoner, J.S., Xueliang, S., Yuan, W., Whitmore, T.J., 1999. Paleoclimate of southwestern China for the past 50,000 yr inferred from lake sediment records. *Quaternary Research* 52, 369–380.
- Hu, Y., Marwick, B., Zhang, J.-F., Rui, X., Hou, Y.-M., Yue, J.-P., Chen, W.-R., Huang, W.-W., Li, B., 2019. Late Middle Pleistocene Levallois stone-tool technology in southwest China. *Nature* 565, 82–85.
- Huang, W., Hou, Y., Si, X., 1997. Stone industry from Panxian Dadong, a cave-site of southeastern China. *Acta Anthropologica Sinica* 16, 171–192.
- Huntley, D.J., Godfrey-Smith, D.I., Thewalt, M.L.W., 1985. Optical dating of sediments. *Nature* 313, 105–107.
- Jacobs, Z., Duller, G.A.T., Wintle, A.G., 2006. Interpretation of single grain  $D_e$  distributions and calculation of  $D_e$ . *Radiation Measurements* 41, 264–277.
- Ji, X., 2008. The fascination of Dahe cave: disclosure of Dahe cave Paleolithic site in Fuyuan. *Chinese Cultural Relics* 6, 78–83.
- Kaifu, Y., Izuho, M., Goebel, T., 2015. Modern human dispersal and behavior in Paleolithic Asia: summary and discussion. In: Kaifu, Y., Izuho, M., Goebel, T., Sato, H., Ono, A. (Eds.), *Emergence and Diversity of Modern Human Behavior in Paleolithic Asia*. Texas A&M University Press, College Station, pp. 535–566.
- Karkanas, P., Schepartz, L.A., Miller-Antonio, S., Wang, W., Huang, W., 2008. Late Middle Pleistocene climate in southwestern China: inferences from the stratigraphic record of Panxian Dadong Cave, Guizhou. *Quaternary Science Reviews* 27, 1555–1570.
- Kreutzer, S., Schmidt, C., Fuchs, M.C., Dietze, M., Fischer, M., Fuchs, M., 2012. Introducing an R package for luminescence dating analysis. *Ancient TL* 30, 1–8.
- Leng, J., 2001. *Early Paleolithic Technology in Eastern and Southern Asia*. Archaeopress, Oxford, UK.
- Li, B., Jacobs, Z., Roberts, R.G., 2016. Investigation of the applicability of standardised growth curves for OSL dating of quartz from Haa Fteah cave, Libya. *Quaternary Geochronology* 35, 1–15.
- Li, B., Jacobs, Z., Roberts, R.G., Galbraith, R., Peng, J., 2017. Variability in quartz OSL signals caused by measurement uncertainties: problems and solutions. *Quaternary Geochronology* 41, 11–25.
- Li, B., Jacobs, Z., Roberts, R.G., Li, S.-H., 2014. Review and assessment of the potential of post-IR IRSL dating methods to circumvent the problem of anomalous fading in feldspar luminescence. *Geochronometria* 41, 178–201.
- Li, B., Roberts, R.G., Jacobs, Z., Li, S.-H., 2015. Potential of establishing a 'global standardised growth curve' (gSGC) for optical dating of quartz from sediments. *Quaternary Geochronology* 27, 94–104.
- Li, F., Kuhn, S.L., Chen, F., Wang, Y., Southon, J., Peng, F., Shan, M., Wang, C., Ge, J., Wang, X., Yun, T., Gao, X., 2018. The easternmost Middle Paleolithic (Mousterian) from Jinsitai Cave, North China. *Journal of Human Evolution* 114, 76–84.
- Li, H., Li, Z., Gao, X., Kuman, K., Sumner, A., 2019. Technological behavior of the early Late Pleistocene archaic humans at Lingjing (Xuchang, China). *Archaeological and Anthropological Sciences* 11, 3477–3490.
- Li, Y., Wen, B., 1986. *Guanyindong: A Lower Paleolithic Site at Qianxi County, Guizhou Province*. Cultural Relics Publishing House, Beijing.
- Li, Y.H., Hou, Y.M., Boëda, E., 2009. Mode of débitage and technical cognition of hominids at the Guanyindong site. *Chinese Science Bulletin* 54, 3864–3871.
- Lisiecki, L.E., Raymo, M.E., 2005. A Pliocene-Pleistocene stack of 57 globally distributed benthic  $\delta^{18}\text{O}$  records. *Paleoceanography* 20, PA1003.
- Liu, W., Martínón-Torres, M., Cai, Y., Xing, S., Tong, H., Pei, S., Sier, M.J., et al., 2015. The earliest unequivocally modern humans in southern China. *Nature* 526, 696–699.
- Liu, W., Wu, X., Pei, S., Wu, X., Norton, C.J., 2010. Huanglong Cave: a Late Pleistocene human fossil site in Hubei Province, China. *Quaternary International* 211, 29–41.
- Lycett, S.J., Norton, C.J., 2010. A demographic model for Palaeolithic technological evolution: the case of East Asia and the Movius Line. *Quaternary International* 211, 55–65.
- Macaulay, V., Hill, C., Achilli, A., Rengo, C., Clarke, D., Meehan, W., Blackburn, J., Semino, O., Scozzari, R., Cruciani, F., Taha, A., Shaari, N.K., Raja, J.M., Ismail, P., Zainuddin, Z., Goodwin, W., Bulbeck, D., Bandelt, H.-J., Oppenheimer, S., Torroni, A., Richards, M., 2005. Single, Rapid Coastal Settlement of Asia Revealed by Analysis of Complete Mitochondrial Genomes. *Science* 308, 1034–1036.
- Martínón-Torres, M., Wu, X., Bermúdez de Castro, J. M., Xing, S., Liu, W., 2017. *Homo sapiens* in the Eastern Asian Late Pleistocene. *Current Anthropology* 58, S434–S448.
- Miller-Antonio, S., Schepartz, L.A., Karkanas, P., Yamei, H., Weiwen, H., Bekken, D., 2004. Lithic raw material use at the Late Middle Pleistocene site of Panxian Dadong. *Asian Perspectives* 43, 314–332.
- Murray, A.S., Wintle, A.G., 2000. Luminescence dating of quartz using an improved single-aliquot regenerative-dose protocol. *Radiation Measurements* 32, 57–73.
- Norton, C.J., Gao, X., Feng, X., 2009. The East Asian Middle Paleolithic reexamined. In: Camps, M., Chauhan, P. (Eds.), *Sourcebook of Paleolithic Transitions: Methods, Theories, and Interpretations*. Springer, New York, pp. 245–254.
- Olley, J.M., Roberts, R.G., Yoshida, H., Bowler, J.M., 2006. Single-grain optical dating of grave-infill associated with human burials at Lake Mungo, Australia. *Quaternary Science Reviews* 25, 2469–2474.
- Otte, M., Weiwen, H., Hu, Y., Hou, Y., 2017. Panxian Dadong et le Levallois chinois. *L'Anthropologie* 121, 255–269.
- Peng, J., Dong, Z., Han, F., Long, H., Liu, X., 2013. R package numOSL: numeric routines for optically stimulated luminescence dating. *Ancient TL* 31, 41–48.
- Peng, J., Li, B., 2017. Single-aliquot regenerative-dose (SAR) and standardised growth curve (SGC) equivalent dose determination

- in a batch model using the R package 'numOSL'. *Ancient TL* 35, 32–53.
- Peng, J., Pagonis, V., Li, B., 2016. On the intrinsic accuracy and precision of the standardised growth curve (SGC) and global-SGC (gSGC) methods for equivalent dose determination: a simulation study. *Radiation Measurements* 94, 53–64.
- Petraglia, M., Korisettar, R., Boivin, N., Clarkson, C., Ditchfield, P., Jones, S., Koshy, J., et al., 2007. Middle Paleolithic assemblages from the Indian subcontinent before and after the Toba supereruption. *Science* 317, 114–116.
- Petraglia, M.D., Haslam, M., Fuller, D.Q., Boivin, N., Clarkson, C., 2010. Out of Africa: new hypotheses and evidence for the dispersal of *Homo sapiens* along the Indian Ocean rim. *Annals of Human Biology* 37, 288–311.
- Prescott, J.R., Hutton, J.T., 1994. Cosmic-ray contributions to dose rates for luminescence and ESR dating: large depths and long-term time variations. *Radiation Measurements* 23, 497–500.
- Preusser, F., Degering, D., Fuchs, M., Hilgers, A., Kadereit, A., Klasen, N., Krbetschek, M., Richter, D., Spencer, J., 2008. Luminescence dating: basics, methods and applications. *Quaternary Science Journal* 57, 95–149.
- Prüfer, K., Racimo, F., Patterson, N., Jay, F., Sankararaman, S., Sawyer, S., Heinze, A., et al., 2014. The complete genome sequence of a Neanderthal from the Altai Mountains. *Nature* 505, 43–49.
- Qiu, Z., Zhang, Y., 1985. Human tooth and Paleoliths found at locality 2 of Longtanshan, Chenggong, Kunming. *Acta Anthropologica Sinica* 4, 233–241.
- R Core Team, 2016. *R: A Language and Environment for Statistical Computing*. R Foundation for Statistical Computing, Vienna, Austria.
- Rhodes, E.J., 2011. Optically stimulated luminescence dating of sediments over the past 200,000 years. *Annual Review of Earth and Planetary Sciences* 39, 461–488.
- Roberts, H.M., Duller, G.A.T., 2004. Standardised growth curves for optical dating of sediment using multiple-grain aliquots. *Radiation Measurements* 38, 241–252.
- Roberts, R.G., Galbraith, R.F., Yoshida, H., Laslett, G.M., Olley, J.M., 2000. Distinguishing dose populations in sediment mixtures: a test of single-grain optical dating procedures using mixtures of laboratory-dosed quartz. *Radiation Measurements* 32, 459–465.
- Roberts, R.G., Jacobs, Z., Li, B., Jankowski, N.R., Cunningham, A.C., Rosenfeld, A.B., 2015. Optical dating in archaeology: thirty years in retrospect and grand challenges for the future. *Journal of Archaeological Science* 56, 41–60.
- Ruan, Q.J., Liu, J.H., Hu, Y., Li, B., Yang, C.C., Luo, X.R., 2017. A study of stone artifacts found in the Tianhuadong Paleolithic site, Heqing, Yunnan. *Acta Anthropologica Sinica* 36, 1–16.
- Stringer, C.B., Andrews, P., 1988. Genetic and fossil evidence for the origin of modern humans. *Science* 239, 1263–1288.
- Thomsen, K.J., Murray, A.S., Buylaert, J.P., Jain, M., Hansen, J.H., Aubry, T., 2016. Testing single-grain quartz OSL methods using sediment samples with independent age control from the Bordes-Fitte rockshelter (Roches d'Abilly site, central France). *Quaternary Geochronology* 31, 77–96.
- Wang, W., Liu, J., Hou, Y., Si, X., Huang, W., Schepartz, L.A., Miller-Antonio, S., 2004. Panxian Dadong, South China: establishing a record of Middle Pleistocene climatic changes. *Asian Perspectives* 43, 302–313.
- Westaway, K.E., Louys, J., Awe, R.D., Morwood, M.J., Price, G.J., Zhao, J.-x., Aubert, M., et al., 2017. An early modern human presence in Sumatra 73,000–63,000 years ago. *Nature* 548, 322–325.
- Wintle, A.G., 1997. Luminescence dating: laboratory procedures and protocols. *Radiation Measurements* 27, 769–817.
- Wintle, A.G., 2008. Luminescence dating of Quaternary sediments – introduction. *Boreas* 37, 469–470.
- Wu, M., Wang, L., Zhang, Y., Zhang, S., 1975. Fossil human teeth and associated cultural relic from Tongzi, Guizhou Province. *Vertebrata Palasiatica* 13, 14–23.
- Zhu, Z., Ji, X., 2010. Study on the stone artifacts from the Laohu Cave Paleolithic site, Baoshan County, Yunnan. *Research of China's Frontier Archaeology* 2010-00, 1–8.